The Journal of Chemical Physics

RESEARCH ARTICLE | JANUARY 24 2024

Vibrational mode-specificity in the dynamics of the OH^- + CH_3I multi-channel reaction FREE

Domonkos A. Tasi ; Gábor Czakó

J. Chem. Phys. 160, 044305 (2024)
https://doi.org/10.1063/5.0189561

The Journal of Chemical Physics ARTICLE pubs.aip.org/aip/jcp

Vibrational mode-specificity in the dynamics of the $OH^- + CH_3I$ multi-channel reaction

Cite as: J. Chem. Phys. 160, 044305 (2024); doi: 10.1063/5.0189561
Submitted: 29 November 2023 • Accepted: 25 December 2023 •
Published Online: 24 January 2024

Domonkos A. Tasi[a] and Gábor Czakó[a]

AFFILIATIONS

MTA-SZTE Lendület Computational Reaction Dynamics Research Group, Interdisciplinary Excellence Centre and Department of Physical Chemistry and Materials Science, Institute of Chemistry, University of Szeged, Rerrich Béla tér 1, Szeged H-6720, Hungary

[a]Authors to whom correspondence should be addressed: dtasi@chem.u-szeged.hu and gczako@chem.u-szeged.hu

ABSTRACT

We report a comprehensive characterization of the vibrational mode-specific dynamics of the $OH^- + CH_3I$ reaction. Quasi-classical trajectory simulations are performed at four different collision energies on our previously-developed full-dimensional high-level *ab initio* potential energy surface in order to examine the impact of four different normal-mode excitations in the reactants. Considering the 11 possible pathways of $OH^- + CH_3I$, pronounced mode-specificity is observed in reactivity: In general, the excitations of the OH^- stretching and CH stretching exert the greatest influence on the channels. For the S_N2 and proton-abstraction products, the reactant initial attack angle and the product scattering angle distributions do not show major mode-specific features, except for S_N2 at higher collision energies, where forward scattering is promoted by the CI stretching and CH stretching excitations. The post-reaction energy flow is also examined for S_N2 and proton abstraction, and it is unveiled that the excess vibrational excitation energies rather transfer into the product vibrational energy because the translational and rotational energy distributions of the products do not represent significant mode-specificity. Moreover, in the course of proton abstraction, the surplus vibrational energy in the OH^- reactant mostly remains in the H_2O product owing to the prevailing dominance of the direct stripping mechanism.

INTRODUCTION

Regulating reactions under controlled conditions is a fundamental objective in chemistry. Since the second half of the 20th century, the substantial progress of computational chemistry has facilitated progressively extensive and in-depth investigations on the dynamics of chemical reactions,[1,2] notably focusing on the mode-specific behavior.[3] The scope of the mode-specific dynamics studies of the ion–molecule reaction types in the gas phase, such as bimolecular nucleophilic substitution (S_N2), is still somewhat lacking in contrast to the atom–molecule reactions.[3–11] However, in the case of the $X^- + CH_3Y$ [X, Y = F, Cl, Br, I] S_N2 reactions, a few mode-specific theoretical and experimental examinations were carried out utilizing quasi-classical trajectory (QCT) simulations,[12–15] quantum dynamics method,[13,16–20] as well as kinetic,[21] spectroscopic[22,23] and crossed-beam ion-imaging measurements.[15] Reduced dimensionality wave packet dynamics calculations were reported for $Cl^- + CH_3I$ by Kowalewski *et al.*[24] and showed that the excitation of the CI stretching mode provides the most significant increase in the reactivity of the S_N2 channel. For $Cl^- + CH_3Br$, Schmatz *et al.*[18] performed quantum dynamics calculations suggesting the probable involvement of the CH stretching in the S_N2 channel, which was formerly considered a spectator mode. In cases of $F^- + CH_3Cl/CH_3I$, collaborative studies involving our group revealed that the CCl/CI stretching and CH_3 umbrella excitations have the most pronounced impact on S_N2, while the CH stretching excitation promotes the corresponding proton-abstraction channel.[13,15] Following these examinations, more detailed experimental investigations were carried out for $F^- + CH_3I$ regarding the influence of the symmetric CH stretching excitation on the dynamics of S_N2, proton abstraction and two other less-probable halide-abstraction channels of $FI^- + CH_3$ and $FHI^- + CH_2$.[25,26] Moreover, it is also notable that the mode-specific dynamics of the $F^- + CHD_2Cl$ and $F^- + CH_3CH_2Cl$ reactions were characterized by our group.[12,27]

Exploring more complex systems is crucial to broadening our understanding of the S_N2 reactions. Therefore, in the past 20–30

years, more emphasis has been placed on investigating S_N2 reactions that include di- or polyatomic nucleophiles (e.g., OH^-, SH^-, CN^-, NH_2^-, and PH_2^-).[28–47] The mechanisms of these S_N2 reactions can be even more complex enabling novel, previously unidentified reaction routes and pathways.[30,31,33,48] In 2002, direct dynamics simulations for the S_N2 reaction between OH^- and CH_3F performed by Hase and co-workers unveiled that the post-reaction H-bonded $CH_3OH\cdots F^-$ global minimum is avoided in the product channel.[41] Since then, several other theoretical studies confirmed the role of the $CH_3OH\cdots F^-$ deep well in dynamics.[49–51] Furthermore, a novel oxide ion substitution was uncovered, which led to the formation of $HF + CH_3O^-$ products.[52–54] By utilizing the crossed-beam ion imaging technique,[55] Wester and co-workers examined the S_N2 reactions of $OH^- + CH_3I$ and $CN^- + CH_3I$.[48,56–59] To explore the dynamics and kinetics of the $OH^- + CH_3I$ S_N2 reaction, direct dynamics simulations were also carried out in Refs. 57 and 60, selected ion flow tube technique was applied in Ref. 61, and the influences of the microsolvation on dynamics were considered in Refs. 56 and 62–65. In 2020, eight different analytical *ab initio* potential energy surfaces (PESs) were constructed for $OH^- + CH_3I$ using the ROBOSURFER program package in order to analyze the impact of the employed levels of theory.[66,67] The methodology test concluded that the most promising opponent for single-point calculations is a composite method based on the Brueckner coupled cluster approach.[68] In collaboration with the Wester group, the present authors reported a detailed theoretical–experimental dynamical characterization for the vibrationally ground-state reaction of $OH^- + CH_3I$.[69] The QCT simulations and the crossed-beam measurements were performed at the same initial translational energies (collision energies, E_{coll} = 11.5, 23.1, 34.6, and 46.1 kcal/mol) and computations revealed 11 distinct reaction pathways, while experimentally, three product ions were detected. In conclusion, a satisfactory agreement was found between theory and experiment. Recently, Rao and Wang[70] fulfilled a quantum dynamics study on the S_N2 pathway of the $OH^- + CH_3I$ reaction using our analytical PES with an application of a reduced-dimensional four-degree-of-freedom dynamics model treating the three H atoms of CH_3I as one pseudo atom. For the ground-state reaction, the computed integral cross sections (ICSs) of the quantum dynamics simulations were in excellent agreement with our previous QCT data. The examination of two vibrational excitations was also implemented, exposing that the CI stretching excitation enhances the reactivity, while, in contrast to the $F^- + CH_3Cl/CH_3I$ cases, the excitation of the CH_3 vibration mode inhibits the S_N2 reaction.

In the present work, following our previous studies and the recently-reported reduced-dimensional quantum dynamics simulations,[66,69,70] we investigate the mode-specificity of the title reaction in a much more comprehensive manner considering all of the possible 11 different paths. We excite four selected vibrational modes of the OH^- and CH_3I reactants and perform QCT simulations on our previously-developed full-dimensional high-level *ab initio* PES applying the same E_{coll} as in the QCT examination of the ground-state reaction[69] in order to describe the effects of the initial vibrational excitations on the reaction dynamics. Thus, our main aim is to assess how different types of excitations impact the reaction probabilities and the energy distributions of the products for the two dominant reaction routes of S_N2 and proton abstraction.

COMPUTATIONAL DETAILS

QCT simulations are performed at E_{coll} of 11.5, 23.1, 34.6, and 46.1 kcal/mol for the $OH^- + CH_3I$ reaction on our PES, which was previously developed using the in-house ROBOSURFER program package.[66,67] The influence of the one-quantum excitations of four different reactant normal modes is considered [v_3 CI stretching (1.61), v_2 CH_3 umbrella (3.53), v_1 symmetric CH stretching (8.77), and v_{OH^-} OH^- stretching (10.55), with the fundamental harmonic energies obtained on the PES and given in kcal/mol in parentheses] in comparison with the results of the unexcited ground-state case, which are derived from Ref. 69. The representative motions of the selected normal mode vibrations are shown in Fig. 1. At the beginning of the trajectories, the zero-point energies (ZPE) and the different vibrational mode excitations of the reactants are prepared by standard normal-mode sampling and the rotational angular momenta are set to zero. The initial orientations of the reactants are randomly chosen and the initial distance of the center of masses of the OH^- and CH_3I reactants is 40 bohr with a given impact parameter (b). For each different excitation, 5000 trajectories are run at each b. Moreover, at each E_{coll}, b is scanned from 0 to b_{max} (where the possibility of the reactive trajectories becomes 0) and the step size is 0.5 bohr. The trajectories are propagated with a time step of 0.0726 fs until the longest atom–atom distance becomes larger than the longest initial one by 1 bohr.

The ICSs of the possible pathways are calculated by a b-weighted numerical integration of the opacity function [$P(b)$, reaction probabilities of the reaction pathways as a function of b],

$$ICS = 2\pi \int_0^{b_{max}} P(b)\, b\, db, \tag{1}$$

employing the trapezoidal rule for the numerical integration,

$$ICS = \pi \sum_{k=1}^{k_{max}} [b_k - b_{k-1}][b_k P(b_k) + b_{k-1} P(b_{k-1})], \tag{2}$$

where the range [0, b_{max}] is divided into k_{max} equidistant parts and b_k = 0.5k bohr (k = 0, 1, 2, …, k_{max}). To consider product ZPE

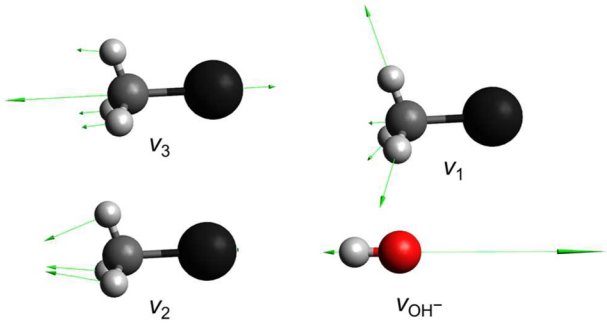

FIG. 1. Schematic representation of the normal-mode vibrations of the reactants (CH_3I and OH^-) studied in the present work: v_3 CI stretching, v_2 CH_3 umbrella, v_1 symmetric CH stretching, and v_{OH^-} OH^- stretching, where v_x [x = 1, 2, 3] refer to the standard Mulliken notations.

violation, two different ZPE constraints are used: (1) soft and (2) hard. In case of (1), those trajectories are accepted, where the sum of the classical vibrational energies of the products is higher than the sum of their ZPEs on the PES, and in case of (2), those trajectories are considered, where the vibrational energies of both products are higher than the corresponding ZPEs on the present PES. The initial attack angle (α) is the angle of the velocity vector of the corresponding reactant and an interatomic vector assigned as the O–H bond for OH^- and the C–I bond for CH_3I. The scattering angle (θ) is the angle of the relative velocity vectors of the center of masses of the reactants and products. The distributions of α and θ are determined by binning the cosine of α and θ into ten equidistant bins from −1 to 1, where cos(θ) = 1 corresponds to forward scattering, and for OH^-, cos(α) = 1(−1) identifies that OH^- approaches CH_3I with its H-side (O-side), while for CH_3I, cos(α) = 1(−1) signifies that CH_3I attacks OH^- with its I-side (C-side). Note that, in the case of proton abstraction, the cosine of θ is binned into 20 equidistant bins. In the present work, B-spline functions are applied for the curve fitting of the calculated data. For the distinction of the possible pathways, the same procedure is applied as in Ref. 69.

RESULTS AND DISCUSSION

The schematic representation of the S_N2 and proton-abstraction pathways along the stationary points is shown in Fig. 2. The benchmark energies[32,69] of the structures are compared with the corresponding PES values, and as it can be seen, the PES reproduces the benchmark data within chemical accuracy (1 kcal/mol) in nearly all cases. Note that the examined four single-excited vibrational energy levels of the OH^- and CH_3I reactants determined on the PES are also depicted in Fig. 2. S_N2 can proceed through three different pathways: the submerged back-side attack Walden inversion with a nontraditional H-bonded transitional state of HTS (−16.65 kcal/mol) as well as the less feasible front-side attack and double-inversion routes, which result in the retention of the initial CH_3I configuration.[71] Proton abstraction has three distinct transition states (TS1′, TS1″, and TS2); however, TS1′and TS1″ are only conformational isomers and both are below HTS. The global minimum is located at the H-bonded PostHMIN complex with a classical energy of −78.78 kcal/mol. Considering the reaction energies of S_N2 and proton abstraction, S_N2 is substan-

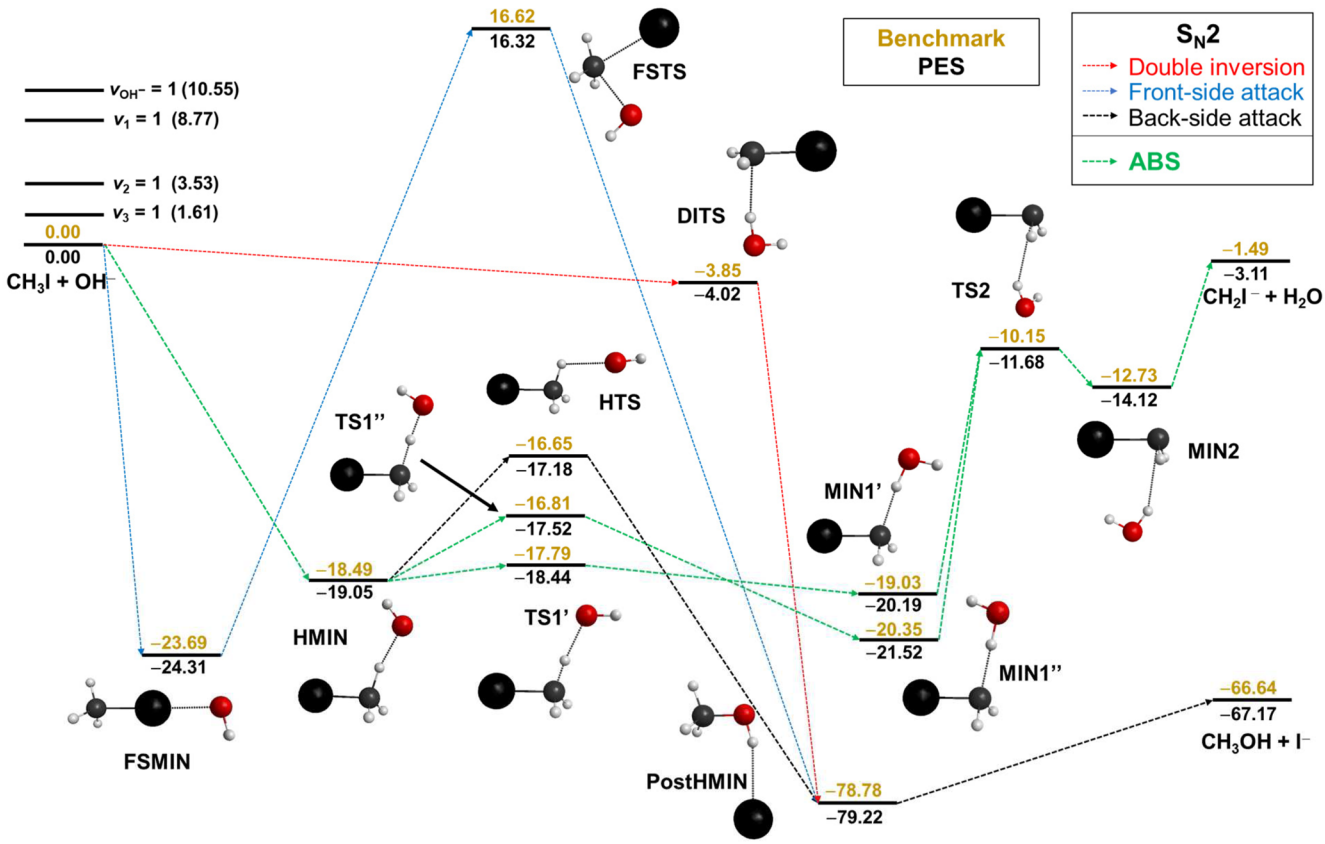

FIG. 2. The schematic potential energy diagram of the S_N2 and proton-abstraction pathways of the $OH^- + CH_3I$ reaction comparing benchmark classical relative energies[32] of the stationary points with the values calculated on our previously-developed PES.[66,69] Four single-excited vibrational energy levels of the reactants obtained on the PES are shown as well.

tially more endothermic (−66.64 kcal/mol) than proton abstraction (−1.49 kcal/mol).

QCT computations are carried out at E_{coll} = 11.5, 23.1, 34.6, and 46.1 kcal/mol for OH^- + CH_3I, and as shown in Fig. 1, in order to compare the results with the unexcited case, a particular normal vibrational mode is excited with one quantum at the start of the simulations.[69] The ICSs of S_N2 and proton abstraction (with/without applying the ZPE constraints) as a function of E_{total} (E_{total} = initial translational + vibrational energy) and E_{coll}, as well as the ratios of ICSs of the excited- and ground-state OH^- + CH_3I reactions are presented in Fig. 3. It is notable that for each vibrational mode, the ZPE restrictions are ineffective for the S_N2 pathway in nearly all instances: For the examined excitations of CH_3I (ν_1, ν_2, and ν_3), a small, negligible ZPE violation can be obtained at E_{coll} = 46.1 kcal/mol. The pathways of S_N2 and proton abstraction are exothermic and barrier-less, and thus their ICSs suffer a major decline as E_{coll} (E_{total}) increases. Considering the E_{total} dependence for S_N2, interestingly, it appears that the spectator vibrational modes of the OH^- stretching and CH stretching have the most pronounced enhancements on the reactivity, as shown in Fig. 3. This phenomenon emerges from the fact that, since these two modes require higher excitation energies, the relative quantity of the initial translational energy within total energy is smaller compared to the other excitations. Therefore, the relatively lower amount of the initial translational energy in the cases of these higher frequency excitations leads to higher reactivity in S_N2. At E_{total} = ~22 kcal/mol, the ν_{OH^-}-excited ICS of S_N2 is almost four times larger than the ground-state ICS, while at higher E_{total} of ~45 kcal/mol, the former ICS values are almost the same. For proton abstraction at lower E_{total}, comparable increases in the ICSs can be observed, as well. Moreover, the employed ZPE constraints enhance the reactivity of proton abstraction more significantly, an increase of over 600% can be eventuated among the hard-restricted mode-specific ICS values. It should also be noted that as E_{coll} increases, the vibrational enhancement decreases in accordance with the reduced time of the possible interaction between the OH^- and CH_3I reactants. The excitations of the OH^- stretching and CH stretching vibrational modes have a similar impact on the ICS values of proton abstraction with and without soft restrictions; however, considering hard restrictions, the proton-abstraction ICSs of the OH^- stretching are notably

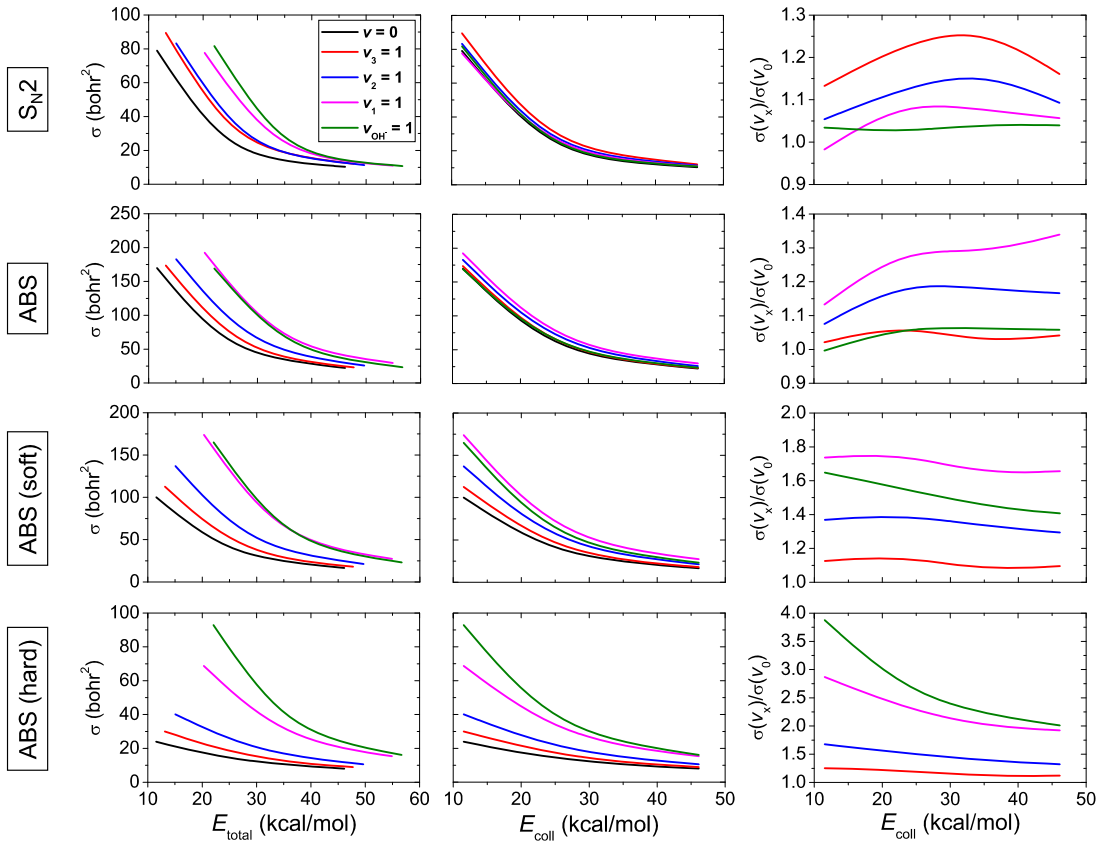

FIG. 3. Mode-specific integral cross-sections of S_N2 and proton abstraction without as well as with soft and hard ZPE restrictions as a function of total energy (collision energy + vibrational excitation energy, first column) and collision energy (second column) and the ratios of the corresponding integral cross sections of the $OH^-(v_{OH^-} = 0)$ + $CH_3I(v_x = 1)$ and the $OH^-(v_{OH^-} = 1)$ + $CH_3I(v_x = 0)$, x = 3, 2, 1, reactions with respect to the ground-state $OH^-(v_{OH^-} = 0)$ + $CH_3I(v = 0)$ reaction as a function of collision energy (third column).

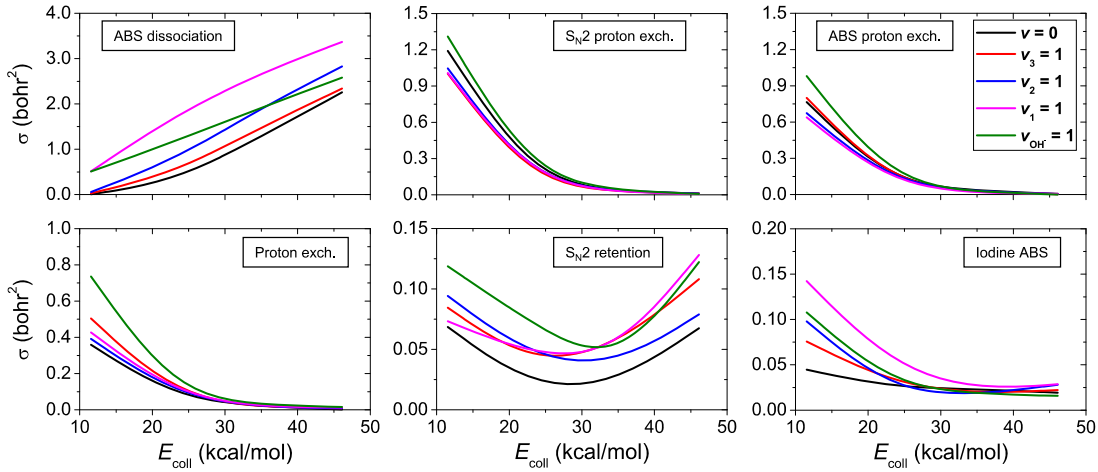

FIG. 4. Mode-specific integral cross-sections for proton abstraction with dissociation, S_N2 with proton exchange, proton abstraction with proton exchange, proton exchange, S_N2 retention, and iodine abstraction of the $OH^-(v_{OH^-} = 0) + CH_3I(v_x = 0, 1)$, $x = 3, 2, 1$, and $OH^-(v_{OH^-} = 1) + CH_3I(v = 0)$ reactions as a function of collision energy.

higher. By plotting the ICSs as a function of E_{coll}, the reactivity of S_N2 is improved by the CI stretching excitation the most, as expected, owing to the breaking of the C–I bond during the mechanism. This finding is in accordance with the quantum dynamics study of Rao *et al.*,[70] although our computations revealed a promotion of the CH_3 umbrella excitation on the S_N2 reactivity in agreement with the previous QCT results of the $F^- + CH_3Cl/CH_3I$ reactions.[13,15] It is important to highlight that at a lower E_{coll} of 11.5 kcal/mol, the CH stretching excitations inhibit the S_N2 reactivity by about 1.5%. For proton abstraction, the CH stretching excitation is the most efficient for enhancing the reactivity due to the C–H bond cleavage in the progress. Nevertheless, as applying ZPE constraints for proton abstraction, the OH^- stretching excitation becomes more dominant in the promotion of the reactivity: By employing soft restrictions, an enhancement of 140%–160% can be recognized for the OH^- stretching compared to the ground-state reaction at each E_{coll}, while in the case of the hard-restricted proton abstraction, the OH^- stretching vibrational mode gains utmost significance among the excitations. The mode-specific ICS values of the possible pathways at each E_{coll} are presented in the supplementary material (Tables S1–S4), and for the ground-state ICSs, see electronic supplementary information of Ref. 69.

In addition to S_N2 and proton abstraction, numerous other possible pathways can be identified for $OH^- + CH_3I$ as discussed in Ref. 69: proton exchange ($OH'^- + CH_3I \rightarrow HOH' + CH_2I^- \rightarrow OH^- + CH_2H'I$), proton abstraction with dissociation (following proton abstraction, the C–I bond of CH_2I^- breaks), S_N2 with proton exchange (preceding back-side attack, a proton exchange occurs between the reactants), proton abstraction with proton exchange (preceding proton abstraction, a proton exchange occurs between the reactants), and iodine abstraction (generation of the $[I\cdots OH]^- + CH_3$ products). The mode-specific ICSs of the aforementioned pathways along with the S_N2 retention channel as the function of E_{coll} are shown in Fig. 4. Within proton abstraction with dissociation, four distinct pathways can be exposed and their ICSs are depicted in Fig. 5. In the course of the separation of the double-inversion and front-side attack pathways, we found that the transition-state attack-angle-based approach is not definitive for the $OH^- + CH_3I$ reaction;[72] nonetheless, according to the trajectory simulations, double inversion is the more feasible process at low E_{coll}

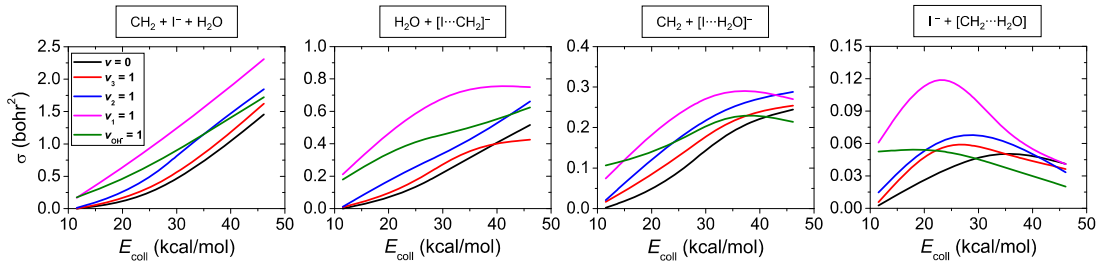

FIG. 5. Mode-specific integral cross-sections for the different types of the proton abstraction with dissociation pathway of the $OH^-(v_{OH^-} = 0) + CH_3I(v_x = 0, 1)$, $x = 3, 2, 1$, and $OH^-(v_{OH^-} = 1) + CH_3I(v = 0)$ reactions as a function of collision energy.

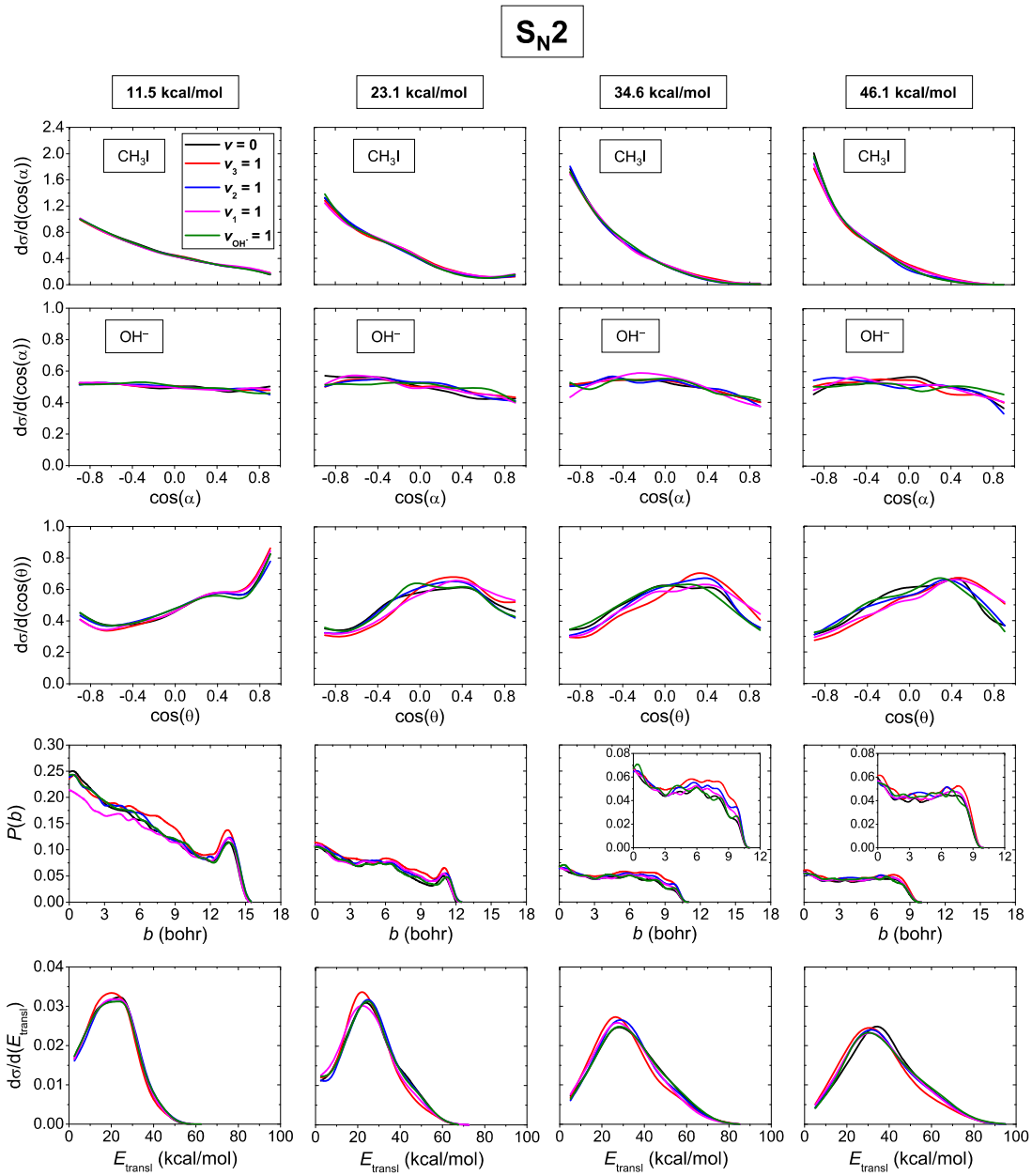

FIG. 6. Normalized initial attack angle (α) distributions of the reactants, normalized scattering angle (θ) distributions of the products, opacity functions [$P(b)$], and the normalized relative translation energy (E_{trans}) distributions of the products for the $OH^-(v_{OH^-} = 0)$ + $CH_3I(v_x = 0, 1)$, $x = 3, 2, 1$, and $OH^-(v_{OH^-} = 1)$ + $CH_3I(v = 0)$ S_N2 reactions at different collision energies.

in agreement with the submerged barrier of DITS (−3.85 kcal/mol). In contrast to F^- + CH_3I, where the CH stretching is clearly the most effective mode for the promotion of double inversion, in the present reaction, the excitation of the OH^- stretching mode happens to be the most preferable choice to facilitate double inversion, as shown in Fig. 4. With an increase in E_{coll}, the probability of the front-side attack pathway increases, resulting in a more substantial impact for the CH stretching and CI stretching vibrational modes. In the case of other pathways involving proton transfer between reactants (S_N2 with proton exchange, proton abstraction with proton exchange, and proton exchange), the largest enhancement is found upon the OH^- stretching excitation as it is coupled to

the reaction coordinate the strongest. Note that certain vibrational excitations inhibit the above-mentioned proton-exchange-involved pathways since they rather promote the competitive S_N2 and proton-abstraction channels. For the channels of proton abstraction with dissociation and iodine abstraction, the excitation of the CH stretching exerts the greatest influence on the reactivity. With regard to the E_{coll} dependence of the mode-specificity of the channels, the ground-state ICSs as well as the corresponding ICS-increasements of the excitations shrink toward higher E_{coll}, excluding proton abstraction with dissociation and S_N2 retention, where the ICSs do not display a decreasing trend as a function of E_{coll}. As seen in Fig. 5, the mode-specific behavior is clearly observable for the four sepa-

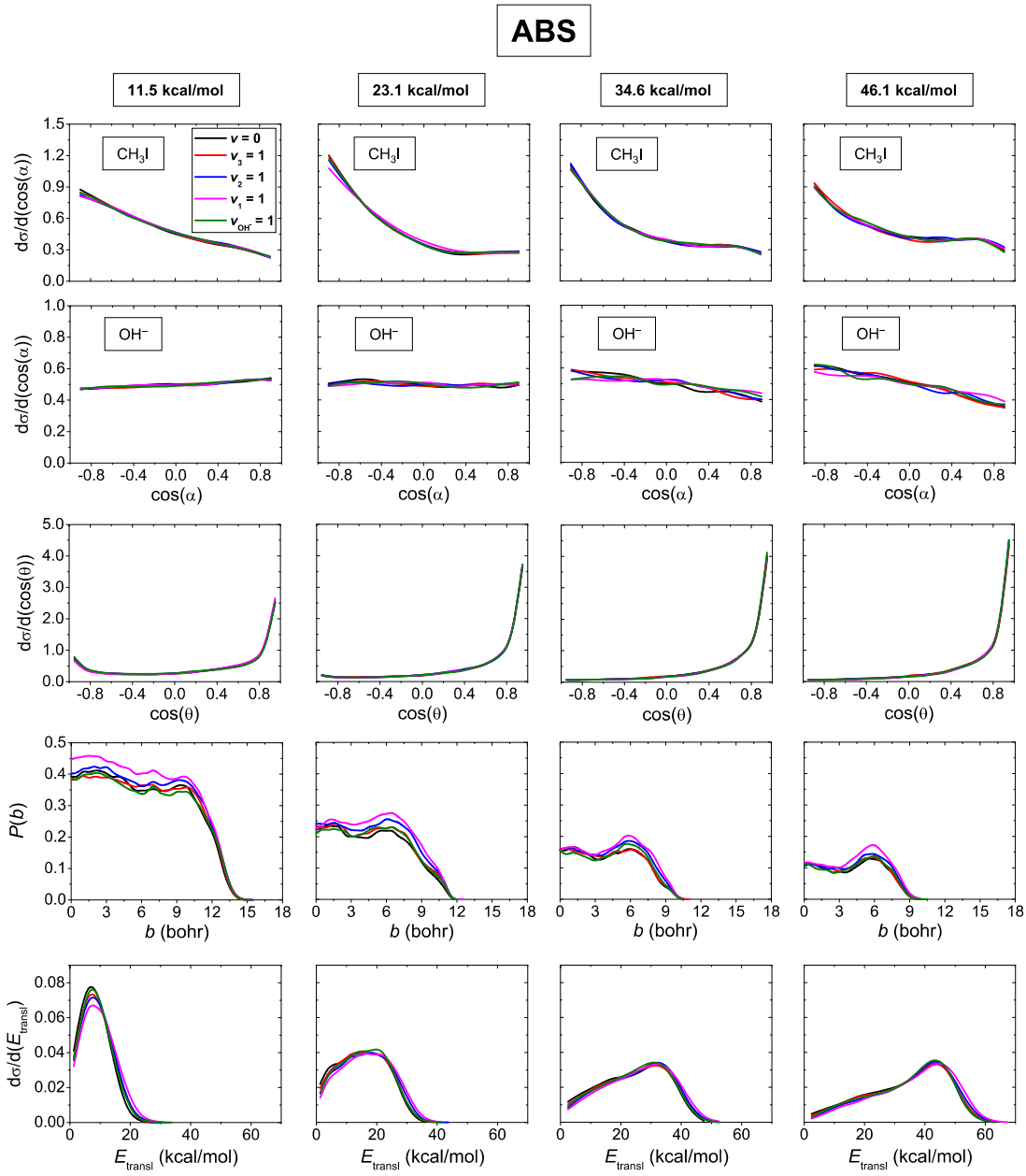

FIG. 7. Normalized initial attack angle (α) distributions of the reactants, normalized scattering angle (θ) distributions of the products, opacity functions [$P(b)$], and the normalized relative translation energy (E_{trans}) distributions of the products for the $OH^-(v_{OH^-} = 0)$ + $CH_3I(v_x = 0, 1)$, $x = 3, 2, 1$, and $OH^-(v_{OH^-} = 1)$ + $CH_3I(v = 0)$ proton-abstraction reactions at different collision energies.

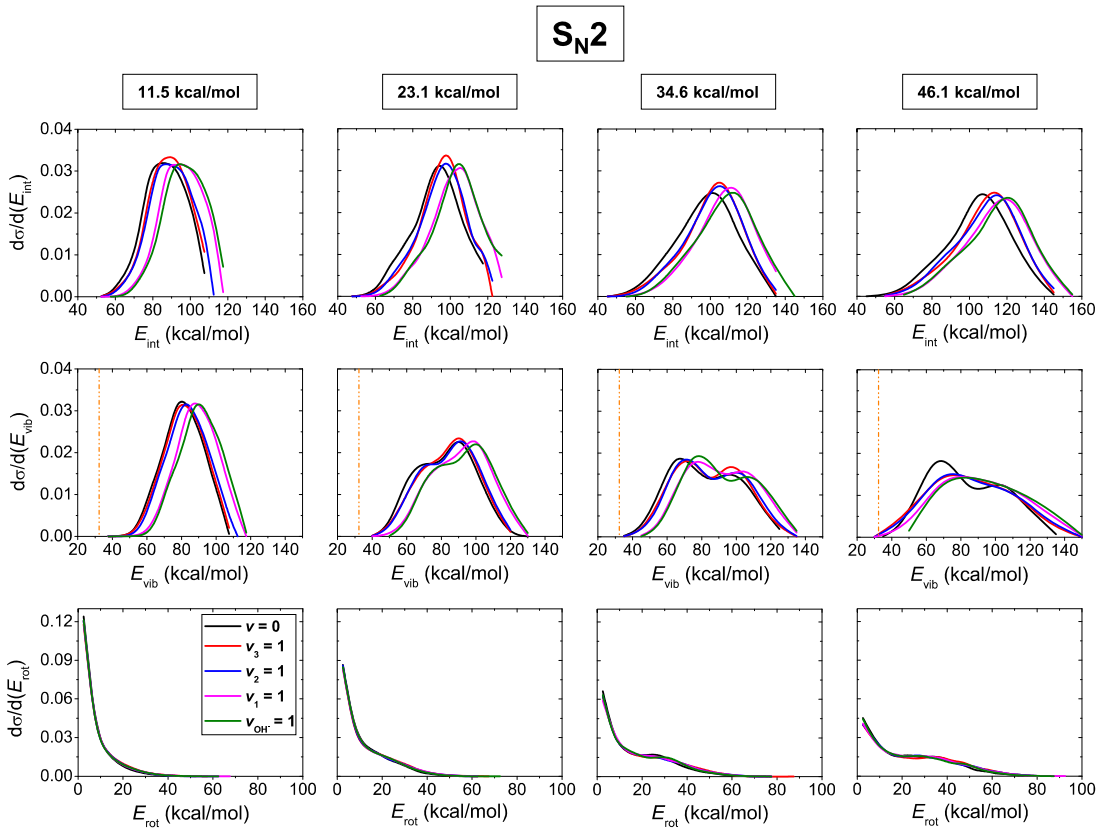

FIG. 8. Normalized internal energy (E_{int}), vibrational energy (E_{vib}), and rotational energy (E_{rot}) distributions of the products for the $OH^-(v_{OH^-} = 0) + CH_3I(v_x = 0, 1)$, $x = 3$, 2, 1, and $OH^-(v_{OH^-} = 1) + CH_3I(v = 0)$ S_N2 reactions at different collision energies. The orange vertical dotted line refers to the zero-point energy of the CH_3OH product (32.37 kcal/mol) on the PES.

rated paths of proton abstraction with dissociation, and almost in all instances, the most prominent effect is seen for the excitation of the CH stretching vibrational mode for each channel. By comparing our results of the title reaction with the crossed-beam measurements performed for $F^- + CH_3I$,[25,26] several similar findings can be stated regarding the influence of the CH stretching excitation. At low E_{coll}, S_N2 is not influenced or even inhibited, and as E_{coll} increases, the CH stretching excitation promotes the reactivity by 5%–10%. In the case of proton abstraction, the enhancement is significant at each E_{coll}. However, in contrast to $F^- + CH_3I$, the iodine-abstraction pathway of $OH^- + CH_3I$ is also enhanced by the CH stretching excitation.

Mode-specific opacity functions as well as the product scattering angle and reactant initial attack angle distributions are plotted at different E_{coll} for the S_N2 and proton-abstraction channels in Figs. 6 and 7, respectively. For S_N2, the promotion of the CI stretching excitation can be more commonly observed at larger b, whereas in the case of smaller b values, the CH stretching excitation hinders the reaction probability at E_{coll} = 11.5 kcal/mol. On the other hand, proton abstraction is enhanced by exciting the CH stretching mode, as discussed earlier, and with increasing E_{coll}, the effect on the reactivity is more pronounced at larger b. It should also be highlighted that the mode-specific character of the b_{max} values is insignificant. Initial attack angle distributions show that, in the case of S_N2 and proton abstraction, CH_3I prefers to attack with its C-side in accordance with the structures of the corresponding transition states (HTS and TS1′, TS1″, respectively), and at higher E_{coll}, this preference is more pronounced, as the indirect character of the pathways is more and more diminishing.[69] Regarding OH^-, the attack angle distributions are rather isotropic. However, it is noteworthy that at E_{coll} = 34.6 and 46.1 kcal/mol, the O-side attack is slightly preferred by proton abstraction in conformity to the gaining dominance of the direct stripping mechanism. In both pathways, for the initial attack angle distributions of the OH^- and CH_3I reactants, only a minor mode-specificity can be identified. With regard to the scattering angle distributions of the products, an apparent forward-scattering and no mode-specificity can be found for proton abstraction, while S_N2 shows a mixed backward/forward-scattering and isotropic pattern, and upon increasing E_{coll}, the CI stretching and CH stretching excitations enhance the generation of the forward-scattered products.

The product relative translation energy distributions of the S_N2 and proton-abstraction pathways at different E_{coll} are presented in Figs. 6 and 7, in order. The internal, vibrational, and rotational

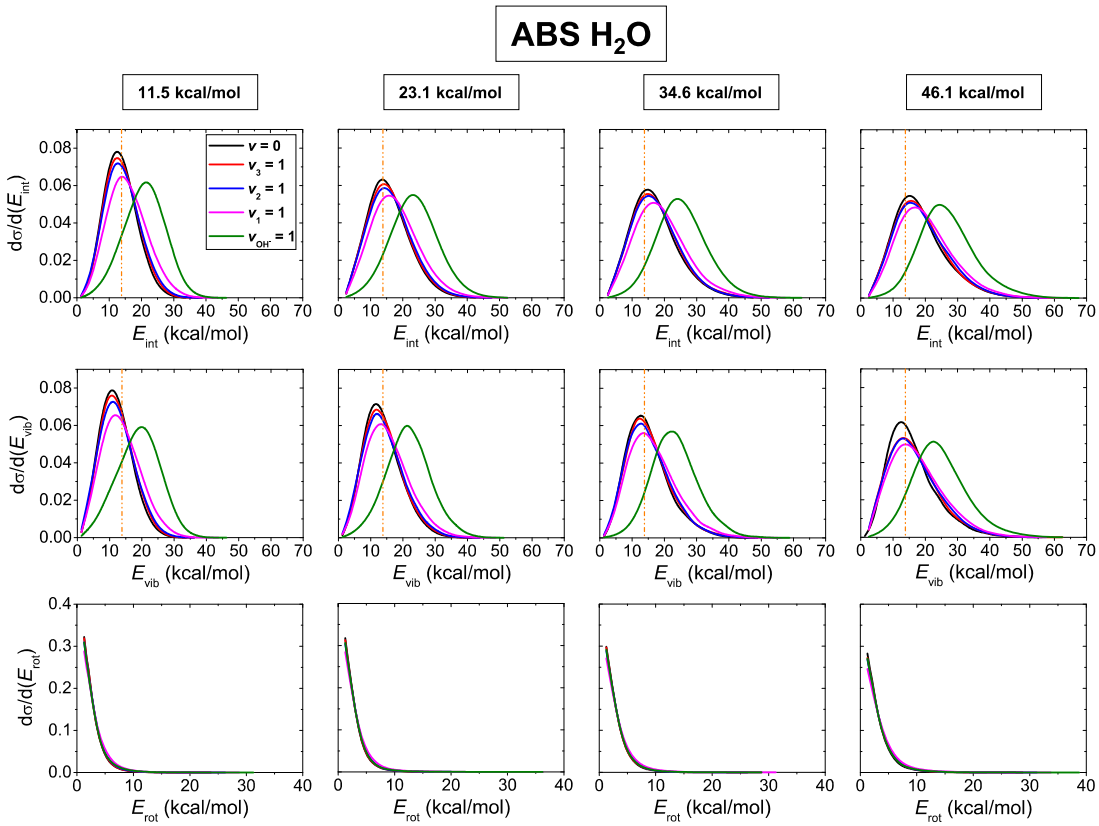

FIG. 9. Normalized internal energy (E_{int}), vibrational energy (E_{vib}), and rotational energy (E_{rot}) distributions of the H_2O product for the $OH^-(v_{OH^-} = 0) + CH_3I(v_x = 0, 1)$, $x = 3, 2, 1$, and $OH^-(v_{OH^-} = 1) + CH_3I(v = 0)$ proton-abstraction reactions at different collision energies. The orange vertical dotted line refers to the zero-point energy of the H_2O product (13.82 kcal/mol) on the PES.

energy distributions of the S_N2 (CH_3OH) and proton-abstraction (H_2O and CH_2I^-) products are given in Figs. 8–10, respectively. In concordance with the product scattering angle distributions, as E_{coll} increases, the translational energy of the proton-abstraction products is more and more impacted signifying the dominance of the direct stripping mechanism, while for S_N2, the post-reaction energy distributions show a rather indirect character.[69] For both pathways, a slight mode-specificity can be observed in the case of the product relative translation energy distributions; however, internal energy distributions have a more significant mode-specific feature showing that the initial vibrational excitation energies evolve into the internal degrees of freedom of the products. Moreover, the product rotational energy distributions have a minor dependence on the vibrational excitations of the reactants, and thus, it can be stated that the energies of the reactant vibrational excitations mostly convert into the vibrational energies of the products. Nevertheless, this picture is more complicated in some instances: For example, the excitation of CH stretching shifts the vibrational energy of the CH_2I^- and H_2O products toward larger energies, but their translation energy distributions marginally broadened as well, and therefore, it can be declared that the excess initial reactant energy is separated between the translational and vibrational energies of the products. With regard to the influence of the OH^- stretching excitation on the H_2O product of proton abstraction, the blue shifts of the internal and vibrational energy distributions are nearly equivalent to the energy of the excitation itself, and thus, in the course of the mechanism, the vibrational energy of the OH^- reactant particularly remains in the H_2O product. Likewise, regarding S_N2, an increase in the internal energy distribution of CH_3OH can be seen for each vibrational excitation and each enhancement is roughly proportional to the energy of the initial vibrational excitation of the reactants. The combination of different indirect mechanisms is also reflected in the post-reaction energy flow for the S_N2 channel: At higher E_{coll}, the vibrational and rotational energy distributions of the CH_3OH product have a two-peak shape suggesting that, in the course of the reaction, the energy is significantly transformed into either the vibrational or the rotational degrees of freedom of the product. Moreover, one can see that as a result of the vibrational excitations, the two-peaked form of the vibrational energy distribution of CH_3OH becomes more flattened at $E_{coll} = 46.1$ kcal/mol.

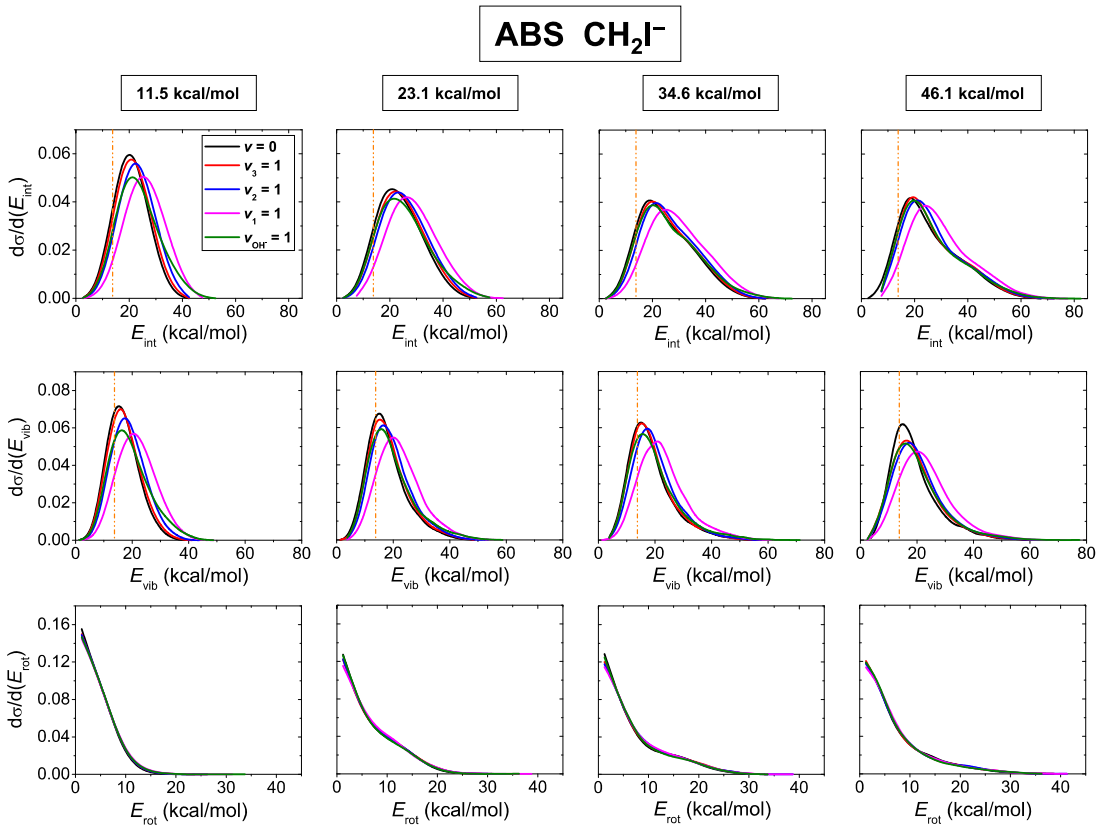

FIG. 10. Normalized internal energy (E_{int}), vibrational energy (E_{vib}), and rotational energy (E_{rot}) distributions of the CH_2I^- product for the $OH^-(v_{OH^-} = 0) + CH_3I(v_x = 0, 1)$, $x = 3, 2, 1$, and $OH^-(v_{OH^-} = 1) + CH_3I(v = 0)$ proton-abstraction reactions at different collision energies. The orange vertical dotted line refers to the zero-point energy of the CH_2I^- product (13.78 kcal/mol) on the PES.

CONCLUSIONS

In this paper, we have performed vibrational mode-specific QCT computations for the seven-atomic $OH^- + CH_3I$ reaction at four different E_{coll} utilizing our previously-developed full-dimensional PES. One-quantum excitations of four different vibrational modes have been considered and their impact on reactivity, mechanism, and energy distribution has been examined. Considering the ICSs as a function of E_{coll}, prominent mode-specificity has been assessed for proton abstraction, especially when ZPE constraints are applied, an increase of over 400% can be recognized in the reactivity. Despite that, the excitations of the vibrational modes have a smaller impact on the ICSs of the S_N2 pathway: The reactant vibrational excitation promotes the reaction by 15%–25% for the CI stretching excitation and by 5%–15% for the other modes, except for the CH stretching excitation at lower E_{coll}, where a minor inhibition of about 1.5% can be seen. In the case of the other possible pathways, a significant mode-specific feature can be obtained, as well. Our findings are consistent with the recently-reported results by Rao and Wang,[70] indicating that the excitations of CI stretching facilitate the S_N2 reaction; however, our QCT results uncovered that the CH_3 umbrella excitation also promotes the reaction. By inspecting the opacity functions of S_N2 and proton abstraction, it can be stated that with increasing E_{coll}, the influence of the most effective excitations is more pronounced at larger b. The mode-specificity of the reactant initial attack angle and product scattering angle distributions is negligible for proton abstraction, while for S_N2 at higher E_{coll}, the CI stretching and CH stretching excitations enhance the generation of the forward-scattered products. For the post-reaction energy distributions, it has been revealed that, in general, the product translational energy distributions have only a minor mode-specificity, and the excess vibrational excitation energies rather flow into the product vibrational energy, because the initial excitations have only a slight effect on the rotational energy of the products.

This work substantiates the fact that even in the case of the submerged-barrier S_N2 reactions, a significant mode-specific character can be unveiled, and for more complex systems, the in-depth theoretical investigation of this phenomenon necessitates the utilization of the QCT method. We hope that our study motivates future theoretical and experimental examinations of the mode-specificity for the seven-atomic $OH^- + CH_3I$ reaction.

SUPPLEMENTARY MATERIAL

See the supplementary material for mode-specific integral cross sections ($bohr^2$) of the possible pathways [S_N2, proton abstraction (with ZPE-constraints), iodine abstraction, S_N2 retention, proton abstraction with proton exchange, S_N2 with proton exchange, proton exchange, and proton abstraction with dissociation ($CH_2 + I^- + H_2O$, $H_2O + [I\cdots CH_2]^-$, $CH_2 + [I\cdots H_2O]^-$, $I^- + [CH_2\cdots H_2O]$)] of the $OH^-(v_{OH^-} = 0) + CH_3I(v_x = 1)$, $x = 3, 2, 1$ and $OH^-(v_{OH^-} = 1) + CH_3I(v = 0)$ reactions.

ACKNOWLEDGMENTS

We acknowledge the financial support of the National Research, Development and Innovation Office–NKFIH, K-125317 and K-146759; Project No. TKP2021-NVA-19 provided by the Ministry of Innovation and Technology of Hungary from the National Research, Development and Innovation Fund, financed under the TKP2021-NVA funding scheme; the National Young Talent Scholarship (Grant No. NTP-NFTÖ-22-B-0050 for D. A. T.); and the Momentum (Lendület) Program of the Hungarian Academy of Sciences.

AUTHOR DECLARATIONS

Conflict of Interest

The authors have no conflicts to disclose.

Author Contributions

Domonkos A. Tasi: Data curation (lead); Formal analysis (lead); Investigation (lead); Methodology (equal); Validation (lead); Visualization (lead); Writing – original draft (lead); Writing – review & editing (lead). **Gábor Czakó**: Conceptualization (lead); Data curation (supporting); Formal analysis (supporting); Funding acquisition (lead); Investigation (supporting); Methodology (equal); Project administration (lead); Resources (lead); Supervision (lead); Validation (supporting); Visualization (supporting); Writing – review & editing (supporting).

DATA AVAILABILITY

The data that support the findings of this study are available from the corresponding authors upon reasonable request.

REFERENCES

[1] T. Hollebeek, T.-S. Ho, and H. Rabitz, Annu. Rev. Phys. Chem. **50**, 537 (1999).
[2] J. M. Bowman and G. C. Schatz, Annu. Rev. Phys. Chem. **46**, 169 (1995).
[3] B. Fu, X. Shan, D. H. Zhang, and D. C. Clary, Chem. Soc. Rev. **46**, 7625 (2017).
[4] S. Yan, Y. T. Wu, B. Zhang, X. F. Yue, and K. Liu, Science **316**, 1723 (2007).
[5] W. Zhang, H. Kawamata, and K. Liu, Science **325**, 303 (2009).
[6] T. Westermann, J. B. Kim, M. L. Weichman, C. Hock, T. I. Yacovitch, J. Palma, D. M. Neumark, and U. Manthe, Angew. Chem., Int. Ed. **53**, 1122 (2014).
[7] W. Yan and D. Wang, Chem. Phys. Lett. **603**, 41 (2014).
[8] R. Welsch and U. Manthe, J. Chem. Phys. **141**, 051102 (2014).
[9] J. Palma and U. Manthe, J. Chem. Phys. **146**, 214117 (2017).
[10] D. Lu and J. Li, Theor. Chem. Acc. **139**, 157 (2020).
[11] J. Lv, J. Yang, D. Zhang, F. Blauert, B. Jiang, D. Dai, W. Zhang, G. Wu, W. Yang, Q. Shuai, and X. Yang, J. Chem. Phys. **159**, 024301 (2023).
[12] I. Szabó and G. Czakó, J. Chem. Phys. **145**, 134303 (2016).
[13] Y. Wang, H. Song, I. Szabó, G. Czakó, H. Guo, and M. Yang, J. Phys. Chem. Lett. **7**, 3322 (2016).
[14] B. Olasz and G. Czakó, J. Phys. Chem. A **122**, 8143 (2018).
[15] M. Stei, E. Carrascosa, A. Dörfler, J. Meyer, B. Olasz, G. Czakó, A. Li, H. Guo, and R. Wester, Sci. Adv. **4**, eaas9544 (2018).
[16] S. Schmatz, ChemPhysChem **5**, 600 (2004).
[17] C. Hennig and S. Schmatz, J. Chem. Phys. **121**, 220 (2004).
[18] C. Hennig and S. Schmatz, J. Chem. Phys. **122**, 234307 (2005).
[19] C. Hennig and S. Schmatz, Chem. Phys. Lett. **446**, 250 (2007).
[20] C. Hennig and S. Schmatz, Phys. Chem. Chem. Phys. **14**, 12982 (2012).
[21] A. A. Viggiano, R. A. Morris, J. S. Paschkewitz, and J. F. Paulson, J. Am. Chem. Soc. **114**, 10477 (1992).
[22] D. S. Tonner and T. B. McMahon, J. Am. Chem. Soc. **122**, 8783 (2000).
[23] P. Ayotte, J. Kim, J. A. Kelley, S. B. Nielsen, and M. A. Johnson, J. Am. Chem. Soc. **121**, 6950 (1999).
[24] M. Kowalewski, J. Mikosch, R. Wester, and R. De Vivie-Riedle, J. Phys. Chem. A **118**, 4661 (2014).
[25] T. Michaelsen, B. Bastian, P. Strübin, J. Meyer, and R. Wester, Phys. Chem. Chem. Phys. **22**, 12382 (2020).
[26] T. Michaelsen, B. Bastian, A. Ayasli, P. Strübin, J. Meyer, and R. Wester, J. Phys. Chem. Lett. **11**, 4331 (2020).
[27] V. Tajti and G. Czakó, Phys. Chem. Chem. Phys. **24**, 8166 (2022).
[28] J. D. Evanseck, J. F. Blake, and W. L. Jorgensen, J. Am. Chem. Soc. **109**, 2349 (1987).
[29] J. M. Gonzales, R. S. Cox, S. T. Brown, W. D. Allen, and H. F. Schaefer, J. Phys. Chem. A **105**, 11327 (2001).
[30] J. Xie and W. L. Hase, Science **352**, 32 (2016).
[31] T. A. Hamlin, M. Swart, and F. M. Bickelhaupt, ChemPhysChem **19**, 1315 (2018).
[32] D. A. Tasi, Z. Fábián, and G. Czakó, J. Phys. Chem. A **122**, 5773 (2018).
[33] D. A. Tasi, Z. Fábián, and G. Czakó, Phys. Chem. Chem. Phys. **21**, 7924 (2019).
[34] C. Li, X. Xin, and D. Wang, Phys. Chem. Chem. Phys. **23**, 23267 (2021).
[35] S. Zhao, G. Fu, W. Zhen, L. Yang, J. Sun, and J. Zhang, Phys. Chem. Chem. Phys. **24**, 24146 (2022).
[36] D. A. Tasi and G. Czakó, J. Chem. Phys. **156**, 184306 (2022).
[37] X. Liu, S. Tian, B. Pang, H. Li, and Y. Wu, Phys. Chem. Chem. Phys. **25**, 14812 (2023).
[38] A. Gutal and M. Paranjothy, Phys. Chem. Chem. Phys. **25**, 15015 (2023).
[39] H. Feng, R. Li, Y. Wu, and X. Liu, ChemPhysChem **25**, e202300525 (2023).
[40] J. M. Gonzales, C. Pak, R. S. Cox, W. D. Allen, H. F. Schaefer III, A. G. Császár, and G. Tarczay, Chem. - Eur. J. **9**, 2173 (2003).
[41] L. Sun, K. Song, and W. L. Hase, Science **296**, 875 (2002).
[42] H. Tachikawa, M. Igarashi, and T. Ishibashi, J. Phys. Chem. A **106**, 10977 (2002).
[43] H. Tachikawa and M. Igarashi, Chem. Phys. **324**, 639 (2006).
[44] H. Yin, D. Wang, and M. Valiev, J. Phys. Chem. A **115**, 12047 (2011).
[45] Y. Xu, T. Wang, and D. Wang, J. Chem. Phys. **137**, 184501 (2012).
[46] J. Chen, Y. Xu, and D. Wang, J. Comput. Chem. **35**, 445 (2014).
[47] J. Xie, J. Zhang, and W. L. Hase, Int. J. Mass Spectrom. **378**, 14 (2015).
[48] E. Carrascosa, M. Bawart, M. Stei, F. Linden, F. Carelli, J. Meyer, W. D. Geppert, F. A. Gianturco, and R. Wester, J. Chem. Phys. **143**, 184309 (2015).
[49] L. Sun, K. Song, W. L. Hase, M. Sena, and J. M. Riveros, Int. J. Mass Spectrom. **227**, 315 (2003).
[50] T. Tsutsumi, Y. Ono, Z. Arai, and T. Taketsugu, J. Chem. Theory Comput. **14**, 4263 (2018).
[51] S. R. Hare, L. A. Bratholm, D. R. Glowacki, and B. K. Carpenter, Chem. Sci. **10**, 9954 (2019).
[52] Y. G. Proenza, M. A. F. de Souza, and R. L. Longo, Chem. - Eur. J. **22**, 16220 (2016).

[53]D. A. Tasi and G. Czakó, Chem. Sci. **12**, 14369 (2021).
[54]J. Qin, Y. Liu, and J. Li, J. Chem. Phys. **157**, 124301 (2022).
[55]J. Mikosch, S. Trippel, C. Eichhorn, R. Otto, U. Lourderaj, J. X. Zhang, W. L. Hase, M. Weidemuüller, and R. Wester, Science **319**, 183 (2008).
[56]R. Otto, J. Xie, J. Brox, S. Trippel, M. Stei, T. Best, M. R. Siebert, W. L. Hase, and R. Wester, Faraday Discuss. **157**, 41 (2012).
[57]J. Xie, R. Sun, M. R. Siebert, R. Otto, R. Wester, and W. L. Hase, J. Phys. Chem. A **117**, 7162 (2013).
[58]J. Xie, R. Otto, J. Mikosch, J. Zhang, R. Wester, and W. L. Hase, Acc. Chem. Res. **47**, 2960 (2014).
[59]E. Carrascosa, J. Meyer, and R. Wester, Chem. Soc. Rev. **46**, 7498 (2017).
[60]J. Xie, J. Zhang, R. Sun, R. Wester, and W. L. Hase, Int. J. Mass Spectrom. **438**, 115 (2019).
[61]J. Xie, S. C. Kohale, W. L. Hase, S. G. Ard, J. J. Melko, N. S. Shuman, and A. A. Viggiano, J. Phys. Chem. A **117**, 14019 (2013).
[62]R. Otto, J. Brox, S. Trippel, M. Stei, T. Best, and R. Wester, Nat. Chem. **4**, 534 (2012).
[63]J. Xie, R. Otto, R. Wester, and W. L. Hase, J. Chem. Phys. **142**, 244308 (2015).
[64]J. Xie, X. Ma, J. Zhang, P. M. Hierl, A. A. Viggiano, and W. L. Hase, Int. J. Mass Spectrom. **418**, 122 (2017).
[65]X. Ji, C. Zhao, and J. Xie, Phys. Chem. Chem. Phys. **23**, 6349 (2021).
[66]D. A. Tasi, T. Győri, and G. Czakó, Phys. Chem. Chem. Phys. **22**, 3775 (2020).
[67]T. Győri and G. Czakó, J. Chem. Theory Comput. **16**, 51 (2020).
[68]K. A. Brueckner, Phys. Rev. **96**, 508 (1954).
[69]D. A. Tasi, T. Michaelsen, R. Wester, and G. Czakó, Phys. Chem. Chem. Phys. **25**, 4005 (2023).
[70]S. Rao and D. Wang, Chin. J. Chem. Phys. **36**, 169 (2023).
[71]I. Szabó and G. Czakó, Nat. Commun. **6**, 5972 (2015).
[72]P. Papp, V. Tajti, and G. Czakó, Chem. Phys. Lett. **755**, 137780 (2020).